Spectrochimica Acta Part B 76 (2012) 56–64

Contents lists available at SciVerse ScienceDirect

Spectrochimica Acta Part B

journal homepage: www.elsevier.com/locate/sab

Optimization of operating parameters for inductively coupled plasma mass spectrometry: A computational study☆

Maryam Aghaei *, Helmut Lindner, Annemie Bogaerts

Research group PLASMANT, Department of Chemistry, University of Antwerp, Universiteitsplein 1, B-2610 Wilrijk-Antwerp, Belgium

ARTICLE INFO

Article history:
Received 9 May 2012
Accepted 15 June 2012
Available online 23 June 2012

Keywords:
Inductively coupled plasma mass spectroscopy
Fundamental study
Computational study
Optimization of operating conditions

ABSTRACT

An inductively coupled plasma, connected to a mass spectrometer interface, is computationally investigated. The effect of pressure behind the sampler, injector gas flow rate, auxiliary gas flow rate, and applied power is studied. There seems to be an optimum range of injector gas flow rate for each setup which guaranties the presence and also a proper length of the central channel in the torch. Moreover, our modeling results show that for any specific purpose, it is possible to control that either only the central gas flow passes through the sampler orifice or that it is accompanied by the auxiliary gas flow. It was also found that depending on geometry, the variation of outgoing gas flow rate is much less than the variation of the injector gas flow rate and this causes a slightly higher pressure inside the torch. The general effect of increasing the applied power is a rise in the plasma temperature, which results in a higher ionization in the coil region. However, the negative effect is reducing the length of the cool central channel which is important to transfer the sample substances to the sampler. Using a proper applied power can enhance the efficiency of the system. Indeed, by changing the gas path lines, the power can control which flow (i.e., only from injector gas or also from the auxiliary gas) goes to the sampler orifice. Finally, as also reported from experiments in literature, the pressure behind the sampler has no dramatic effect on the plasma characteristics.

1. Introduction

The inductively coupled plasma (ICP) is by no doubt the most popular ion source in analytical chemistry for elemental mass spectrometry (MS) [1,2]. In ICP-MS a mass spectrometer is coupled to an ICP torch by an interface including sampler and skimmer cones so that representative samples of the plasma can be transmitted through its orifices to the mass analyzer. In recent years, there has been an increased interest in studying the influence of a MS sampler, both upstream [3–11] and downstream [12–15] from the interface cone. However, a detailed comparison of the plasma characteristics with and without sampling interface is only made experimentally by Farnsworth and coworkers [16] and Hieftje and group members [17]. It is found that the insertion of a metal cone interface, which is grounded and cooled, into the high temperature plasma causes changes in the plasma characteristics that affect the analytical performance of ICP-MS.

Besides experimental studies, also computational investigations tried to provide a better insight in the ICP when it is coupled with a MS. An approximate model of ideal gas flow through the sampling cone had been used in the hemispherical-sink model by Douglas and French [18]. Spencer et al. [19,20] applied the so-called Direct Simulation Monte Carlo (DSMC) algorithm to simulate the flow of neutral argon gas through the first vacuum stage of the ICP-MS. The plasma velocity data a few millimeters upstream from the sampler, as obtained from their calculations, were in good correspondence with experiments. However, the upstream density and temperature gradients associated with the cool center and the hot outer region of the gas flow from the ICP torch were not included in their model [19]. Moreover, no plasma was assumed in the model and approximate parameters at the stagnation point had to be provided.

We recently investigated the effect of the presence of a sampler on the fundamental plasma characteristics in ICP-MS [21], based on the model explained in Refs. [22,23]. Both our calculation results and measured data from [16,17] indicated that the upstream plasma temperature and electron density are lowered in the presence of a MS sampler. Moreover, the gas flow entrainment into the sampling orifice has a significant effect on the plasma gas velocity [3,16,21].

The investigations mentioned above [16,17,21] were performed at fixed conditions (i.e. applied power, sampling depth, central gas flow rates, etc.). Because ICP-MS is one of the most important methods for elemental analysis, a large number of investigations were performed to study the effect of ICP operation conditions on the plasma parameters, in order to optimize the analytical performance [24–33]. However, most studies involving ICP-MS operating conditions have focused on their effect on the overall instrument performance and not on the upstream plasma [26–31]. Effects of the rf power, nebulizer

☆ This paper is dedicated to Gary M. Hieftje, on the occasion of his 70th birthday, in recognition of his boundless contributions to spectroscopy and analytical chemistry.

* Corresponding author.
E-mail address: Maryam.aghaei@ua.ac.be (M. Aghaei).

0584-8547/$ – see front matter © 2012 Elsevier B.V. All rights reserved.
doi:10.1016/j.sab.2012.06.006

flow rate, sample composition and torch-shield configuration on the ion-transport efficiency through the ICP-MS interface have been studied via laser-induced fluorescence upstream and downstream from the sampler by Macedone et.al. [24]. The same authors [34] also showed that the barium ion number density in the plasma upstream from the sampler drops as the sampling depth is reduced. In Refs. [32,33], Gamez et al. performed Thomson and Rayleigh scattering measurements using an imagine-based instrument for fundamental plasma studies. It was found that the perturbation in radial distribution of electron density and the drop in gas temperature due to the MS interface change with applied rf power, central gas flow rate and sampling depth [32,33].

Expanding upon our computational work in Ref. [21], the purpose of this study is to systematically investigate the effect of the operating conditions on the upstream plasma characteristics of the ICP in contact with a MS interface. Thus, a wide range of central gas and auxiliary gas flow rates is applied. Moreover, the effect of the pressure downstream the sampler and of the forward power is studied in detail. The temperature profiles, the path lines of the flow inside the coil region as well as in the region close to the MS interface are studied. The calculation results will be compared with measured data from [24,32,33].

2. Description of the model

The simulation setup is thoroughly described in our previous publications [21,22]. A commercial computational fluid dynamics (CFD) program, called Fluent v13.0.0 (ANSYS), was used [35]. For defining the heat capacity and thermal conductivity, a number of self-written modules were added as user-defined functions (UDFs), as described in Ref. [22]. The solver algorithm of the simulation is the so-called coupled algorithm [35]. Except for the injector diameter, which is set to 1.5 mm, the other characteristics of the 2D axisymmetric geometry of the ICP torch are the same as described in detail in Ref. [22]. As explained in Ref. [21], a mass spectrometer interface (sampler) is placed at a distance of 41.5 mm from the gas inlets, on the central axis. The sampler has a central orifice of 1 mm diameter. The downstream pressure of the sampler is fixed to 1 Torr (1.32×10^{-3} atm), unless specified otherwise (i.e., when the effect of this parameter is studied). The ambient gas pressure and exhaust pressure are set to 1 atm and 0.99 atm, respectively. The ICP gas stream and the ambient gas are both assumed to be argon. As discussed in Ref. [22] and verified by comparing the calculation results with experiments in Ref. [21], it is justified to apply the local thermodynamic equilibrium (LTE) condition to the plasma. The plasma species considered in the model are Ar atoms, singly-charged and doubly-charged Ar ions, and electrons. Their transport properties are calculated by kinetic theory, as fully described in Ref. [22]. Since the Reynolds number of the flow, even on the sampler (=115.6), is far from the turbulence regime, the laminar behavior assumption can be utilized to solve the Navier–Stokes equations for the flow inside the torch [35]. The model is validated by experimental work in Refs. [21,23]. The total power coupled to the plasma is set to 1000 W (unless specified otherwise, as in Section 3.3 below) and the frequency of the harmonic external electric current density is 27 MHz. The flow rate of the outer inlet is 12 L min^{-1} and the flow rates of the central and intermediate inlets are varied from 0.3 to 1.4 L/min and from 0.3 to 1.2 L/min in Sections 3.1 and 3.2, respectively.

3. Results and discussion

As mentioned above, the purpose of this paper is to systematically study the effect of pressure behind the sampler, injector gas and auxiliary gas flow rates, and applied power. We have carried out several calculations to investigate the effect of pressure behind the sampler, keeping the injector and auxiliary gas flow rates fixed at 1.0 and 0.4 L/min, respectively. The downstream pressures were varied as 1.32×10^{-3}, 0.5 and 0.75 atm. The results showed no significant change in gas flow path lines and temperature profiles. This corresponds to measurements by Hieftje et al. [32], who also concluded that the pressure behind the interface cone does not affect the plasma characteristics of the ICP torch. In the following, we will therefore focus only on the effect of injector gas and auxiliary gas flow rates and applied power.

3.1. Effect of injector gas flow rate

It is well known that adjustments in the central flow rate will lead to a change in the axial distribution of ions in the ICP [36,37]. The gas flow path lines, originating from the central and outer inlets, colored by velocity in m s^{-1}, are plotted in Fig. 1 at different central gas flow rates, ranging from 0.3 to 1.4 L/min. The path lines originating from the intermediate inlets are colored in black to be distinguishable from the ones of the central and outer gas, and for the sake of further discussions. The flow rate of the gas in the outer and intermediate torch tubes are 12 L/min and 0.4 L/min, respectively.

The formation of a central channel in the ICP torch upon increase of the central gas flow rate can be studied in Fig. 1. In Fig. 1a, no central channel is formed yet and the central flow is not straight at all. By increasing the flow rate of the central injector to 0.35 L/min (see Fig. 1b), a small part of the flow moves directly toward the end of the torch and faces the sampler cone without turning toward the outer sides in the coil region. To explain this, we refer to the so-called "transition flow rate" introduced by Lindner et al. in Ref. [23]. Indeed, for each specific injector inlet diameter, there is a specific transition flow rate below which the central flow does not go straight and does not form a central channel (see Fig. 9 in Ref. [23]). This means that depending on the geometrical setup, the central channel could only be observed above a specific injector gas flow rate (i.e., 0.3 L/min in the current study). Therefore, in order to guide the sample substances efficiently along the torch and toward the mass spectrometer, the injector flow rate should exceed this crucial transition flow rate.

By further increasing the central gas flow rate, the fraction of central path lines which turns toward the outer sides of the torch decreases and a larger fraction of path lines goes straight toward the sampler orifice (see Fig. 1b–f). This trend continues until an injector flow rate of 1.0 L/min (see Fig. 1f), when 100% of the central gas flows in a more or less straight line through the central channel. In Ref. [33], Gamez et al. also demonstrated experimentally that the central channel becomes well-defined only at flow rates above 1.0 L/min.

When the central gas flow rate further increases to 1.2 and 1.4 L/min (see Fig. 1g and h), the central gas stays along the central line; however, a change in the pattern of the auxiliary gas becomes obvious in Fig. 1h, i.e., a part of the auxiliary gas comes closer to the central line. This is studied in detail in Fig. 2, which shows the path lines at still higher flow rates, i.e. 1.6 and 1.8 L/min. The purple contours demonstrate the area of external power coupling. It is clear from Fig. 2a and especially from Fig. 2b that the flow originating from the intermediate inlet passes through a region where the amount of the coupled electrical power is low (i.e., the outer part of the purple contours in Fig. 2). This means that the efficiency of power coupling to the plasma decreases, because the auxiliary gas cannot transfer the external power and heat up the central gas. It is known that a rise in central gas flow rate, at fixed external power, always leads to a lower temperature inside the torch, as will be demonstrated in Fig. 3 below; however, the behavior illustrated in Fig. 2 is the reason why the transport efficiency of aerosol drops for flow rates above 1.4 L/min, as is reported by Macedone et al. [24]. Therefore, our calculations predict that the central flow rate should not exceed 1.4 L/min in order to keep the aerosol transport efficiency

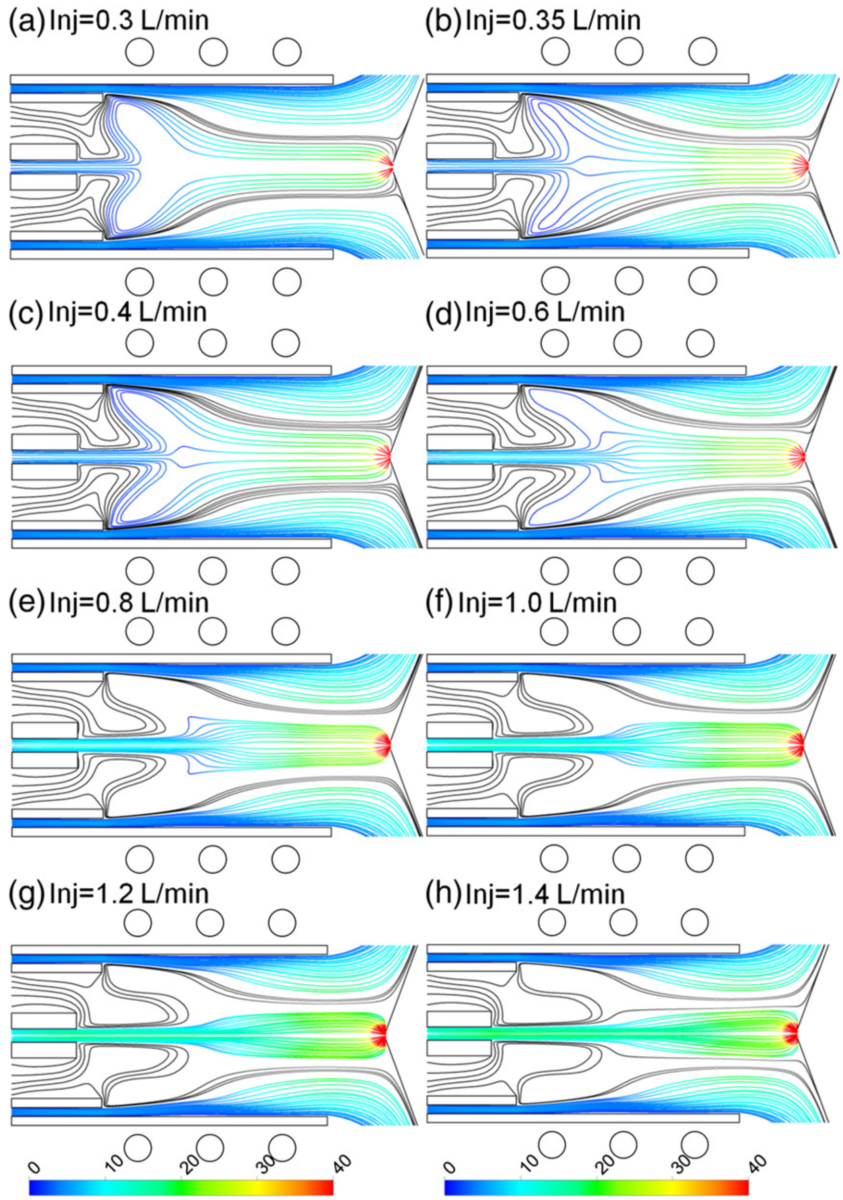

Fig. 1. 2D gas flow velocity path lines originating from the central and outer inlets, colored by velocity in m s^{-1}, and from the intermediate inlet, colored in black, at different central gas flow rates, ranging from 0.3 to 1.4 L/min. The intermediate gas and outer gas flow rates are kept fixed at 0.4 and 1.2 L/min and the power is 1000 W.

acceptable. On the other hand, as discussed above, to ensure that the injector gas entirely flows in a straight line and efficiently guides the sample substances toward the mass spectrometer, the injector gas flow rate should be at least 1.0 L/min. Therefore, our calculations predict that, when the other conditions are fixed (i.e., geometrical setup, auxiliary gas flow rate, power…), the optimum injector gas flow rate is around 1.0–1.2 L/min.

Fig. 3 illustrates the 2D profiles of plasma temperature at different injector gas flow rates, ranging from 0.3 to 1.4 L/min (i.e., the same as in Fig. 1 above). It is indeed obvious that increasing the central gas flow rate yields a general drop in temperature, but simultaneously, the (cooler) central channel becomes more distinguished (see Fig. 3f, g, h). The small black lines above each plot in Fig. 3 indicate the length of the cool central channel, to make this clear. This effect of central gas flow rate on the central channel is in agreement with experiments. Indeed, it was measured in Ref. [33] that a higher central gas flow rate yields a wider central channel.

As illustrated in Ref. [21], the electron density profiles show the same pattern as the temperature profiles, and they are therefore not presented here in 2D plots, to avoid too many figures. However, Fig. 4 presents the electron density in the plasma at the edge of the sampler orifice (i.e. at an axial position of 41.5 mm and at 0.5 mm above the central axis) as a function of injector gas flow rate. Following the behavior of the temperature, the general effect of increasing the injector gas flow rate is a drop in electron density, which is obvious for the flow rates above 0.6 L/min. However, a rise in electron density for the flow rates below 0.6 L/min is observed in Fig. 4. To explain this trend, we refer to the relevant flow path lines in Fig. 1 (i.e. Fig. 1a, b, c, d). It is clear that in these cases, a part of the central gas flow passes through the high power coupling areas (cf. Fig. 2) and directly gets the energy and becomes ionized; however, for the higher flow rates, the central flow is heated up mostly by the heat transferred from the auxiliary gas. Referring to Fig. 2, it can therefore easily be understood why at flow rates above 1.4 L/min, the electron density is too small, as is indeed observed in Fig. 4.

Fig. 5 shows the outgoing gas flow rate from the ICP torch to the mass spectrometer through the sampler orifice, in L/min, for different injector gas flow rates. When the injector gas flow rate increases from

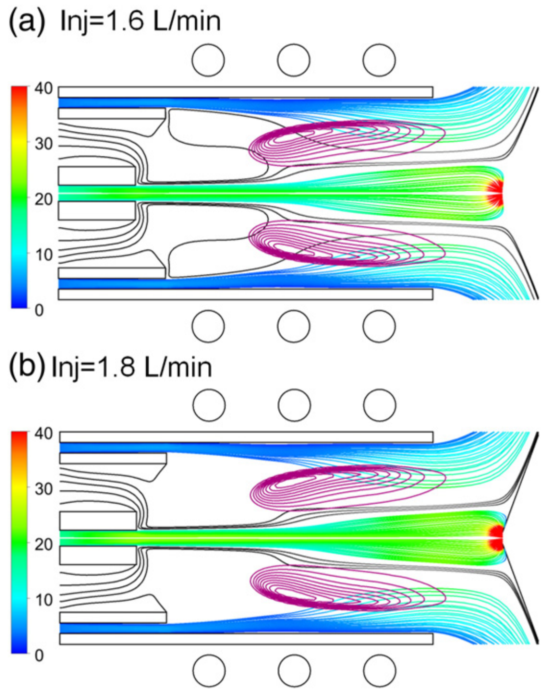

Fig. 2. 2D gas flow velocity path lines originating from the central and outer inlets, colored by velocity in m s^{-1}, and from the intermediate inlet, colored in black, at (a) 1.6 and (b) 1.8 L/min central gas flow rates. The purple contours demonstrate the area of external power coupling. The other conditions are the same as in Fig. 1.

0.3 to 1.4 L/min, the flow rate passing through the sampler orifice only changes from 1.12 to 1.21 L/min. Hence, at fixed conditions of geometry, pressure behind the sampler, etc., changing the injector gas flow rate does not change significantly the flow rate passing through the sampler. This implies that the gas pressure inside the torch should increase, because the amount of flow inserted is increasing while the amount of outgoing flow is almost constant, and hence more gas stays inside the ICP torch. It should be noted that the flow inserted from the central inlet never escapes to the open sides of the torch (see Fig. 1) and the only way of exiting the torch is through the sampler. Fig. 6 presents the pressure inside the ICP torch at different points along the central channel, for different central gas flow rates. The rise of pressure due to the rise in the injector flow rate is confirmed by this figure, and is especially apparent near the gas inlets (i.e., at $x = 0$ mm). In our study, for an orifice of 1 mm diameter and an injector inlet of 1.5 mm diameter, a change in injector flow rate of 1.1 L/min causes only 0.095 L/min change in the outgoing flow rate, and this results in a pressure rise of at maximum about 140 Pa (or 1.4×10^{-3} atm) inside the torch. These values can be different for different geometrical shapes of the ICP.

In order to understand better the behavior of the path lines inside the torch, we will now focus on the path lines going out through the sampler toward the mass spectrometer. As shown in Fig. 1. a–c, for the flow rates up to 0.4 L/min (i.e. 0.3, 0.35, 0.4 L/min), in addition to the central gas, a part of the auxiliary gas also exits through the sampler orifice, while for the higher flow rates (i.e. Fig. 1d–h), only the injector gas can escape through the sampler orifice. This change in the behavior of the auxiliary gas flow can be explained by the ratio of auxiliary gas and injector gas flow rates. In these simulations, the auxiliary flow rate was set to 0.4 L/min. Therefore, it appears that at injector gas flow rates above this value of auxiliary gas flow rate, only the injector gas can escape through the orifice, whereas at injector gas flow rates below or equal to the auxiliary gas flow rate, both the auxiliary and injector gas can pass through the orifice. To investigate this behavior in more detail and to check whether this thumb rule is generally valid, we performed calculations with various auxiliary gas flow rates, as will be presented in the next section.

3.2. Effect of auxiliary gas flow rate

Calculations are performed with various auxiliary gas flow rates, i.e. 0.6, 0.8, and 1.0 L/min, as presented in Fig. 7a, b and c, respectively. The results with auxiliary gas flow rate of 0.4 L/min were presented in Fig. 1 above. In all plots of Fig. 7, the flow originating from the central inlet passes through the sampler orifice, and the flow originating from the outer inlet escapes to the open sides of the torch. Hence, the exit patterns of central and outer flows always stay the same. However, for the intermediate (i.e., auxiliary) gas flow, the pattern is changed, depending on the values of the injector and auxiliary gas flow rates. Indeed, if the injector gas flow rate is lower than or equal to the auxiliary gas flow rate (i.e. Fig. 7a1, a2, b1, b2, c1 and c2), our calculations predict that some part of the auxiliary gas can pass through the sampler cone. On the other hand, when the central gas flow rate is higher than the auxiliary gas flow rate (i.e. Fig. 7a3, b3 and c3), all the auxiliary gas escapes to the open sides of the torch and it does not pass through the sampler. This behavior was observed for all central gas flow rates investigated, i.e., higher than 0.3 L/min and lower than 1.2 L/min.

The behavior is somewhat different for an auxiliary gas flow rate as low as 0.3 L/min or as high as 1.2 L/min, as is illustrated in Fig. 8. Fig. 8a1–a4 shows the flow path lines for an auxiliary gas flow rate of 0.3 L/min. It is indeed clear from these plots that when the auxiliary gas flow rate is 0.3 L/min (or less), some fraction of the auxiliary gas can pass through the orifice even when the injector gas flow rate is higher than the auxiliary gas flow rate (i.e., up to 0.5 L/min; see Fig. 8a3). Only when the injector gas flow rate becomes 0.6 L/min (see Fig. 8a4), the auxiliary gas cannot escape through the orifice anymore. This suggests that for the injector gas flow rates in the range of 0.3–0.5 L/min, the amount of gas flowing through the orifice is too low for filling the orifice, and there is still “room” for some auxiliary gas. If we want to have only the injector gas entering the mass spectrometer, as this gas flow typically contains the sample substances to be analyzed, we should increase the injector gas flow rate to values of 0.6 L/min or higher, as shown in Fig. 8a4. Therefore, by tuning the values of injector gas flow rate and auxiliary gas flow rate, we can control which gas fraction enters the mass spectrometer, and this might be a way to increase the detection efficiency.

On the other hand, when the auxiliary gas flow rate is 1.2 L/min (and more), the auxiliary gas can even not pass through the orifice when the injector gas flow rate is still 0.2 L/min lower than the auxiliary gas flow rate (i.e., 1.0 L/min; see Fig. 8b2), and only the injector gas can enter the mass spectrometer. This suggests that in this range of injector gas flow rate (i.e., 1.0 to 1.4 L/min), the amount of gas originating from the central inlet is high enough to completely fill the orifice and it does not allow any other flow (e.g., originating from the intermediate inlet) to pass through the sampler orifice. Only for an injector gas flow rate of 0.8 L/min or less (see Fig. 8b1), some fraction of the auxiliary gas can pass through the sampler orifice. Again, we can conclude that for each specific geometrical shape, by setting the proper flow rates for the central and auxiliary gas, we can control which gas can escape through the sampler orifice. The sample substances are inserted together with the central gas flow into the torch. If the analyte ion cloud is small, which means that the analytes do not diffuse more than 2–3 mm, i.e., the width of the central gas flow, they are only transported by the central injector gas stream. Therefore, the ion detection efficiency would be higher in the case that only the injector gas passes through the sampler. However, depending on the position upstream the ICP where analyte diffusion starts, the diffusion length can also be larger than the central flow width. This means that some of the analyte ions will also be in

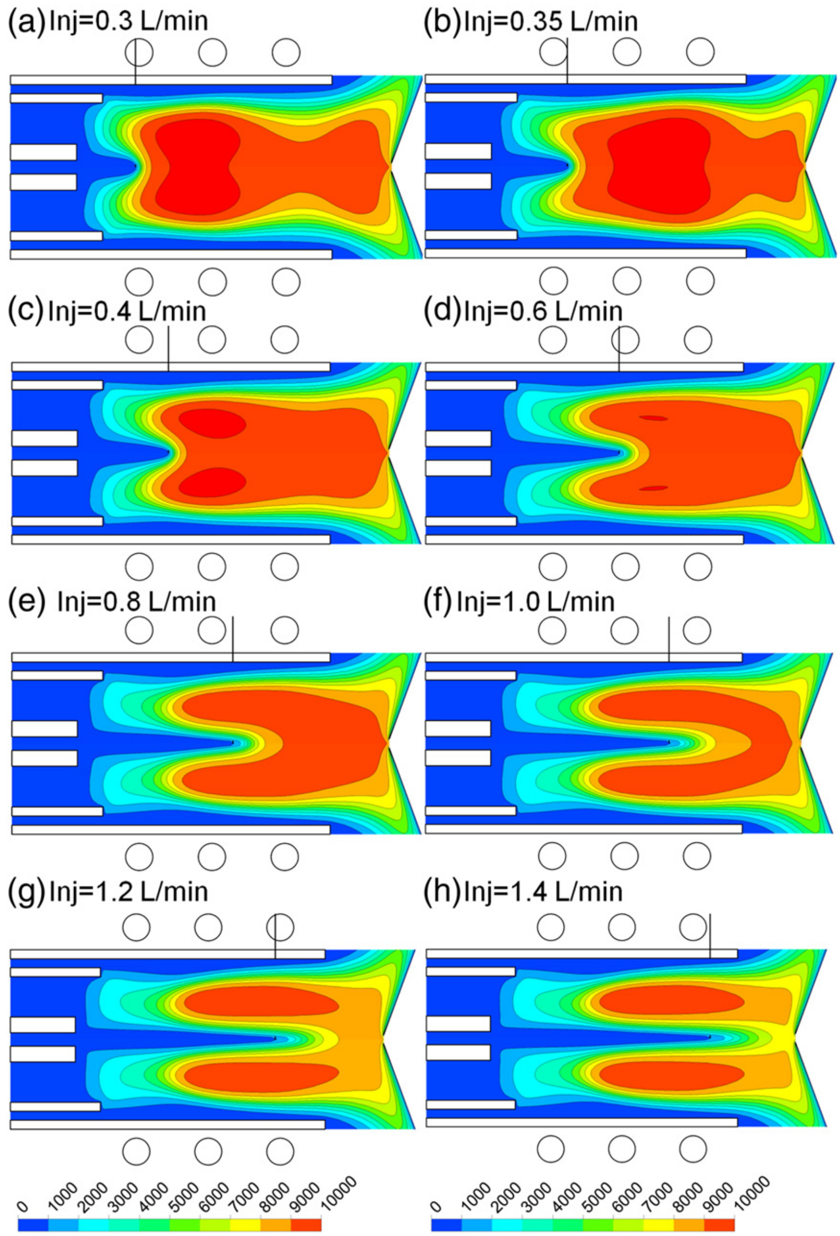

Fig. 3. 2D temperature profiles (K), at different central gas flow rates, ranging from 0.3 to 1.4 L/min. The other conditions are the same as in Fig. 1. The small black lines above each plot indicate the length of the cool central channel.

the auxiliary gas stream, and in that case, it would be better that also (part of) the auxiliary gas can pass through the sampler orifice. It should be noted that the width of the central flow depends on the torch and sampler geometry, especially on the central inlet and the sampler orifice diameter.

3.3. Effect of applied power

To study the effect of the applied power on the plasma characteristics in the ICP, calculations were performed for several values of applied power, i.e., 750, 1000, 1250 and 1500 W. The central gas flow rate is kept fixed at 1 L/min and the flow rate of the outer and intermediate torch tubes are 12 L/min and 0.4 L/min, respectively.

Fig. 9 shows the gas flow path lines, originating from the central and outer inlets, colored by velocity (in m s^{-1}) for different applied powers. Again, the path lines originating from the intermediate inlets are colored in black for better visualization. The purple contours demonstrate the area of maximum external power coupling. It is clear that the shape, size and position of these efficient power coupling regions change by varying the applied power. At 750, 1000 and 1250 W (see Fig. 9a, b, c) the intermediate gas flows entirely through the efficient power coupling areas. On the other hand, at 1500 W (Fig. 9d), the intermediate flow passes through a region with lower coupled power, while most power is transferred to the outer flow. Indeed, by increasing the applied power, the auxiliary gas flow is slightly shifted to the central region of the torch. This behavior was not observed in the absence of the sampler cone [21]. Besides the effect on the auxiliary gas flow path lines, the higher applied power also causes the central flow path lines to expand more rapidly, and this trend was also found to be more significant in the presence of the sampler. Finally, the power also affects the fraction of gas that can pass through the sampler orifice. Indeed, at 750, 1000 and 1250 W, the intermediate gas will entirely escape to the open sides of the ICP torch and only the central flow reaches the sampler orifice. At 1500 W, however, a part of the auxiliary gas, along with the central gas, passes through the sampler orifice. Hence, the gas reaching the sampler is not just the injector

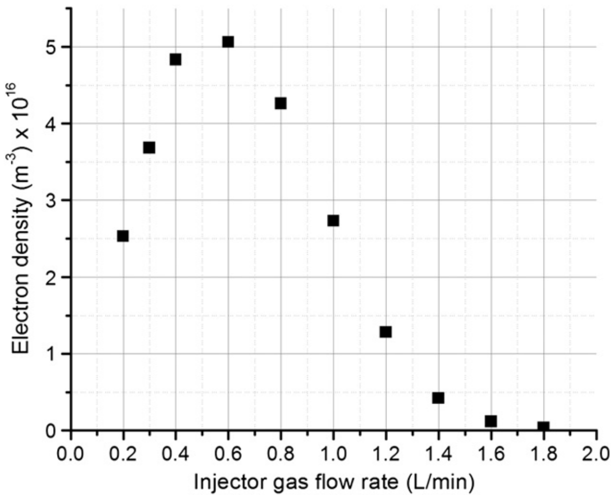

Fig. 4. Electron density (m^{-3}) in the plasma at the edge of the sampler orifice (i.e. at an axial position of 41.5 mm and at 0.5 mm above the central axis) as a function of injector gas flow rate.

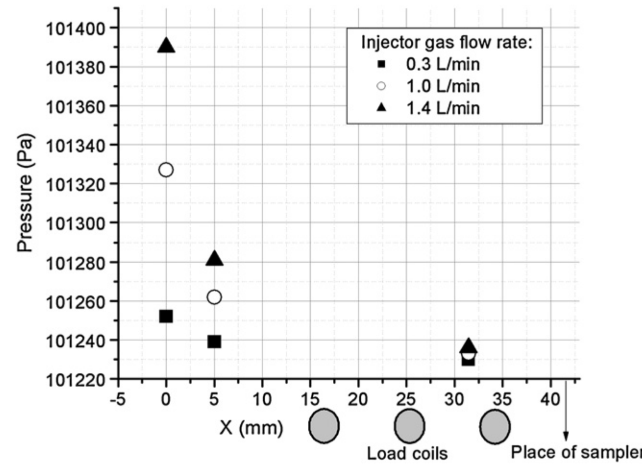

Fig. 6. Pressure (Pa) inside the ICP torch at different points along the central channel, for different injector gas flow rates. The load coils and the place of the sampler are also indicated in this figure, for clarity.

flow which contains the sample substances to be analyzed, and this may lead to a lower detection efficiency. At first sight, it seems surprising that a higher applied power would yield a lower detection efficiency, but it is also reported in Ref. [24] that only a power rise up to 1300 W causes a better transport efficiency while for power values above 1300 W, the transport efficiency decreases, which is in agreement with our computational results.

Another, more expected effect of increasing the power is a temperature rise inside the torch. In Fig. 10, the 2D temperature profiles are depicted at different applied powers. It is obvious that when the temperature inside the coil region increases due to higher power input, this also yields a higher temperature in the rest of the ICP, and therefore the length of the cool central channel decreases slightly, as indicated by the small black lines above each plot. This means that the sample particles should pass through a hotter central channel, which is to be avoided, because a cool central channel is crucial for transferring the sample substances to the sampler. Combining the effect of power on the path lines and the temperature profiles, it can be concluded that a rise in the applied power increases the plasma temperature, which leads to more ionization in the coil region, but on the other hand, it also causes the central channel to become less cool and a bit narrower, which should be avoided (see above).

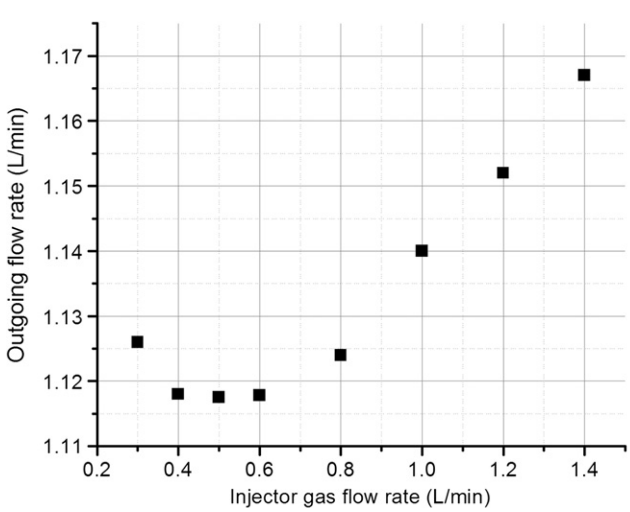

Fig. 5. Outgoing gas flow rate (in L/min) from the ICP torch to the mass spectrometer through the sampler orifice, in L/min, for different injector gas flow rates.

Therefore, our simulations suggest that the applied power should be kept below 1500 W (favorably up to 1250 W). Moreover, a fraction of the auxiliary gas will be able to pass also through the sampler orifice, when the power becomes too high. Again, it depends on the ion cloud diameter compared to the width of the central gas flow whether the latter is beneficial or not (see above). However, as the geometry used in this model is the same as the one used by Farnsworth et al. [24], it seems beneficial for the ICP-MS detection efficiency with the similar geometry as the current work to allow only the central flow passing through the sampler orifice toward the mass spectrometer because a lower detection efficiency is reported in Ref. [24] for the higher coupled power (1500 W), which is the case when the auxiliary gas also passes through the sampler.

4. Conclusion

The effect of pressure behind the sampler, injector gas flow rate, auxiliary gas flow rate, and applied power on the plasma characteristics in an ICP connected to a mass spectrometer is computationally studied, in order to optimize the operating conditions for good analytical practice in ICP-MS. In this model, kinetic theory is applied to the plasma in the whole ICP torch region.

Downstream the sampler, changes in the pressure do not have any noticeable effect on the plasma characteristics such as velocity path lines, temperature and electron density. This is in agreement with experiments from literature.

Our calculations predict that the optimum injector gas flow rate is around 1.0–1.2 L/min for the conditions under study (i.e., geometrical setup, auxiliary gas flow rate, power…). Indeed, to ensure that the injector gas entirely flows in a straight line and efficiently guides the sample substances toward the mass spectrometer, the injector gas flow rate should be at least 1.0 L/min. On the other hand, the injector gas flow rate should not exceed 1.4 L/min, to avoid that the auxiliary gas cannot pass through regions in the plasma with high power coupling and will not be able to transfer the energy efficiently to the injector gas.

It was also observed that when increasing the injector gas flow rate, the outgoing flow rate (i.e., passing through the sampler orifice) does not vary so much, so that a higher central flow rate causes a slightly higher pressure inside the torch.

Furthermore, our calculation results have demonstrated that the injector gas flow rate should be preferentially higher than the auxiliary gas flow rate, to avoid that the auxiliary gas can pass through the sampler orifice, and to ensure that only the injector gas can enter

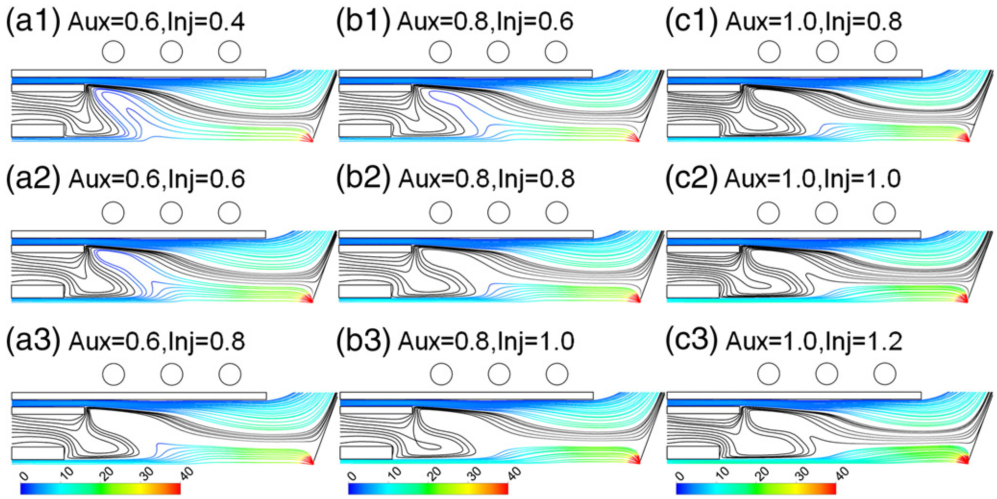

Fig. 7. 2D gas flow velocity path lines originating from the central and outer inlets, colored by velocity in m s^{-1}, and from the intermediate inlet, colored in black, at (a) 0.6, (b) 0.8 and (c) 1.0 L/min of intermediate gas flow rates. The central gas flow rate is (1) lower than, (2) equal to and (3) higher than the intermediate gas flow rate. Only half of the 2D axisymmetric torch is plotted.

the mass spectrometer, which is necessary to optimize the detection efficiency of the sample substances, at least in the case when the ion cloud diameter is small, i.e., when the analyte ions are transported only by the injector gas.

The latter effect can also be achieved by tuning the applied power. Indeed, the applied power affects the gas path lines, and can therefore control which flow (i.e., only the central gas or also the auxiliary gas) can pass through the sampler orifice. Furthermore, depending on the geometry, the general effect of increasing the applied power is a rise in the plasma temperature which results in a higher ionization in the coil region. However, it also results in a reduction of the length of the cool central channel, which is crucial for transferring the sample substances to the sampler. Moreover, at too high power values (~1500 W), the auxiliary gas cannot pass through the high power coupling regions in the plasma anymore, and will not be able to transfer the energy efficiently to the injector gas. Therefore, our calculations predict that the optimum applied power will be in the range of 1000–1250 W at the conditions under study.

Acknowledgments

The authors gratefully acknowledge financial support from the University of Antwerp Methusalem Financing. This work was carried out using the Turing HPC infrastructure at the CalcUA core facility of

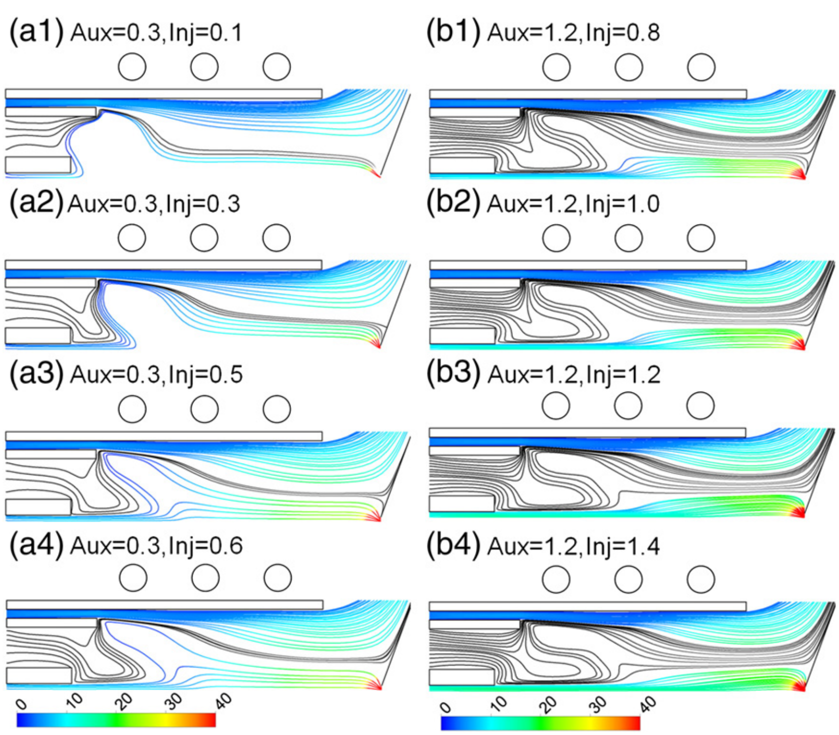

Fig. 8. 2D gas flow velocity path lines originating from the central and outer inlets, colored by velocity in m s^{-1}, and from the intermediate inlet, colored in black, at (a) 0.3 and (b) 1.2 L/min of intermediate gas flow rates and different values of injector gas flow rate. Only half of the 2D axisymmetric torch is plotted.

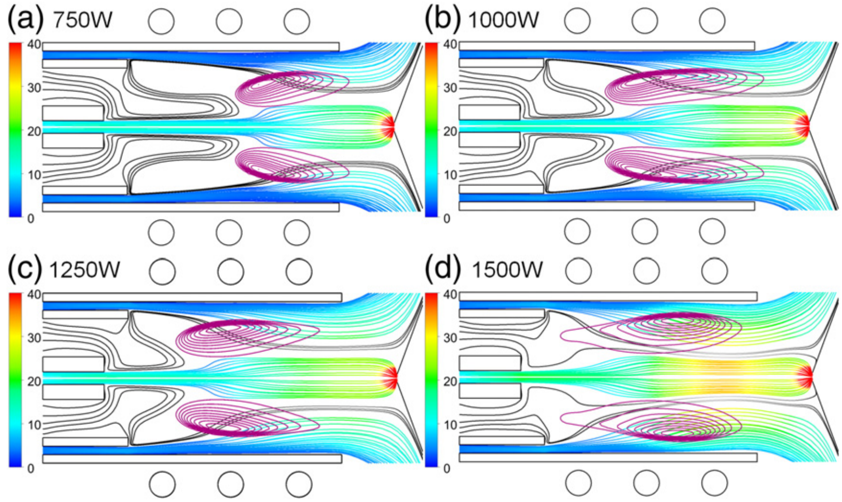

Fig. 9. 2D gas flow velocity path lines originating from the central and outer inlets, colored by velocity in m s^{-1}, and from the intermediate inlet, colored in black, at (a) 750, (b) 1000, (c)1250 and (d) 1500 W of applied power. The injector, auxiliary and outer gas flow rates are kept fixed at 1.0, 0.4 and 1.2 L/min.

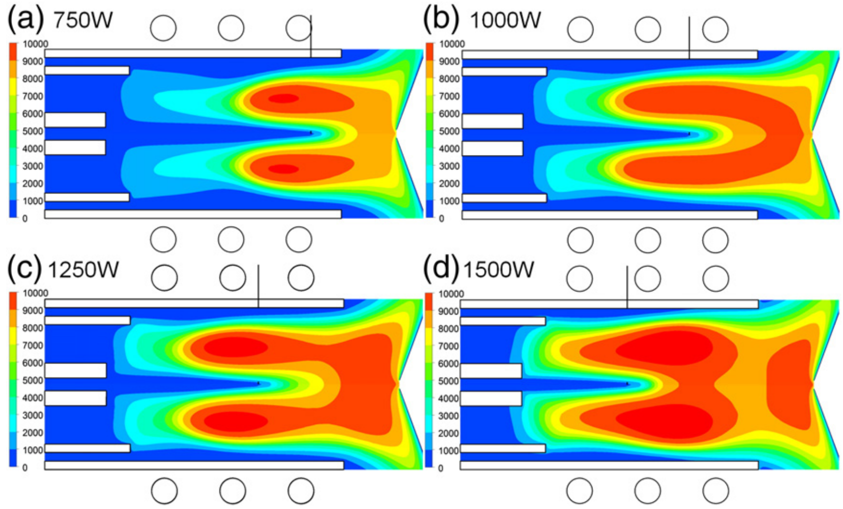

Fig. 10. 2D temperature profile (K), at (a) 750, (b) 1000, (c) 1250 and (d) 1500 W of applied power. The other conditions are the same as in Fig. 9. The small black lines above each plot indicate the length of the cool central channel.

the Universiteit Antwerpen, a division of the Flemish Supercomputer Center VSC, funded by the Hercules Foundation, the Flemish Government (department EWI) and the Universiteit Antwerpen.

References

[1] A. Montaser, Inductively Coupled Plasma Mass Spectrometry, Wiley, New York, 1998.
[2] In: S.J. Hill (Ed.), Inductively Coupled Plasma Spectrometry and its Applications, CRC Press, Boca Raton, 1999.
[3] I.I. Stewart, C.E. Hensman, J.W. Olesik, Influence of gas sampling on analyte transport within the ICP and ion sampling for ICP-MS studied using individual, isolated sample droplets, Appl. Spectrosc. 54 (2000) 164–174.
[4] G. Meyer, R. Foster, A. Van der Hoeff, T. Albert, S. Luan, K. Hu, S. Karpova-Nadel, J. Schmeizel, Increasing laboratory productivity by combining ICP optical emission with ICP mass spectrometry, Am. Lab. 28 (1996) 21–24.
[5] H.P. Longerich, Mass spectrometric determination of the temperature of an argon inductively coupled plasma from the formation of the singly charged monoxide rare earths and their known dissociation energies, J. Anal. At. Spectrom. 4 (1989) 491–497.
[6] K. Lepla, M.A. Vaughan, G. Horlick, Simultaneous atomic emission and mass spectrometric measurements on an inductively coupled plasma, Spectrochim. Acta Part B 46 (1991) 967–973.
[7] R.S. Houk, Y. Zhai, Comparison of mass spectrometric and optical measurements of temperature and electron density in the inductively coupled plasma during mass spectrometric sampling, Spectrochim. Acta Part B 56 (2001) 1055–1067.
[8] R.S. Houk, J.K. Schoer, J.S. Crain, Deduction of excitation temperatures for various analyte species in inductively coupled plasmas from vertically-resolved emission profiles, Spectrochim. Acta Part B 42 (1987) 841–852.
[9] L. Pei-Qi, G. Pei-Zhing, L. Tei-Zheng, R.S. Houk, Langmuir probe measurements of electron temperature in an ICP, Spectrochim. Acta Part B 43 (1988) 273–285.
[10] H. Niu, R.S. Houk, Fundamental aspects of ion extraction in inductively coupled plasma mass spectrometry, Spectrochim. Acta Part B 51 (1996) 779–815.
[11] J.S. Crain, F.G. Smith, R.S. Houk, Mass spectrometric measurement of ionization temperature in an inductively coupled plasma, Spectrochim. Acta Part B 45 (1990) 249–259.
[12] B.S. Duersch, P.B. Farnsworth, Characterization of the ion beam inside the skimmer cone of an inductively coupled plasma mass spectrometer by laser excited atomic and ionic fluorescence, Spectrochim. Acta Part B 54 (1999) 545–555.
[13] D.M. Chambers, G.M. Hieftje, Fundamental studies of the sampling process in an inductively coupled plasma mass spectrometer. II. Ion kinetic energy measurements, Spectrochim. Acta Part B 46 (1991) 761–784.
[14] A.L. Gray, R.S. Houk, J.G. Williams, Langmuir probe potential measurements in the plasma and their correlation with mass spectral characteristics in inductively coupled plasma mass spectrometry, J. Anal. At. Spectrom. 2 (1987) 13–20.
[15] R.S. Houk, J.K. Schoer, J.S. Crain, Plasma potential measurements for inductively coupled plasma mass spectrometry with a center-tapped load coil, J. Anal. At. Spectrom. 2 (1987) 283–286.
[16] H. Ma, N. Taylor, P.B. Farnsworth, The effect of the sampling interface on spatial distributions of barium ions and atoms in an inductively coupled plasma ion source, Spectrochim. Acta Part B 64 (2009) 384–391.
[17] S.A. Lehn, K.A. Warner, M. Huang, G.M. Hieftje, Effect of an inductively coupled plasma mass spectrometry sampler interface on electron temperature, electron

number density, gas–kinetic temperature and analyte emission intensity upstream in the plasma, Spectrochim. Acta Part B 57 (2002) 1739–1751.
[18] D.J. Douglas, J.B. French, Gas dynamics of the inductively coupled plasma mass spectrometry interface, J. Anal. At. Spectrom. 3 (1988) 743–747.
[19] R.L. Spencer, J. Krogel, J. Palmer, A. Payne, A. Sampson, W. Somers, C.N. Woods, Modeling the gas flow upstream and in the sampling nozzle of the inductively coupled plasma mass spectrometer via the Direct Simulation Monte Carlo algorithm, Spectrochim. Acta Part B 64 (2009) 215–221.
[20] R.L. Spencer, N. Taylor, P.B. Farnsworth, Comparison of calculated and experimental flow velocities from the sampling cone of an inductively coupled plasma mass spectrometer, Spectrochim. Acta Part B 64 (2009) 921–924.
[21] M. Aghaei, H. Lindner, A. Bogaerts, Effect of a mass spectrometer interface on inductively coupled plasma characteristics: a computational study, J. Anal. At. Spectrom. 27 (2012) 604–610.
[22] H. Lindner, A. Bogaerts, Multi-element model for the simulation of inductively coupled plasmas: effects of helium addition to the central gas stream, Spectrochim. Acta Part B 66 (2011) 421–431.
[23] H. Lindner, A. Murtazin, S. Groh, K. Niemax, A. Bogaerts, Simulation and experimental studies on plasma temperature, flow velocity and injector diameter effects for an inductively coupled plasma, Anal. Chem. 83 (2011) 9260–9266.
[24] J.H. Macedone, D.J. Gammon, P.B. Farnsworth, Factors affecting analyte transport through the sampling orifice of an inductively coupled plasma mass spectrometer, Spectrochim. Acta Part B 56 (2001) 1687–1695.
[25] B.S. Duersch, Y. Chen, A. Ciocan, P.B. Farnsworth, Optical measurements of ion density in the second vacuum stage of an inductively coupled plasma mass spectrometer, Spectrochim. Acta Part B 53 (1998) 569–579.
[26] S. Kaneco, T. Nomizo, T. Tanaka, N. Mizutani, H. Kawaguchi, Optimization of operating conditions in individual airborne particle analysis by inductively coupled plasma mass spectrometry, Anal. Sci. 11 (1995) 835–840.
[27] W.G. Diegor, H.P. Longerich, Parameter interaction in signal optimization of an ICP mass spectrometer, At. Spectrosc. 21 (2000) 111–117.
[28] H.P. Longerich, B.J. Fryer, D.F. Strong, C.J. Kantipuly, Effects of operating conditions on the determination of the rare earth elements by inductively coupled plasma-mass spectrometry (ICP-MS), Spectrochim. Acta Part B 42 (1987) 75–92.
[29] S.E. Long, R.M. Brown, Optimization in inductively coupled plasma mass spectrometry, Analyst (Cambridge, United Kingdom) 111 (1986) 901–906.
[30] Q. Xie, R. Kerrich, Optimization of operating conditions for improved precision of zirconium and hafnium isotope ratio measurement by inductively coupled plasma mass spectrometry (ICP-MS), J. Anal. At. Spectrom. 10 (1995) 99–103.
[31] B.T.G. Ting, M. Janghorbani, Optimization of instrumental parameters for the precise measurement of isotope ratios with inductively coupled plasma mass spectrometry, J. Anal. At. Spectrom. 3 (1988) 325–336.
[32] G. Gamez, S.A. Lehn, M. Huang, G.M. Hieftje, Effect of mass spectrometric sampling interface on the fundamental parameters of an inductively coupled plasma as a function of its operating conditions. Part I. Applied RF power and vacuum, Spectrochim. Acta Part B 62 (2007) 357–369.
[33] G. Gamez, S.A. Lehn, M. Huang, G.M. Hieftje, Effect of mass spectrometric sampling interface on the fundamental parameters of an inductively coupled plasma as a function of its operating conditions. Part I. Applied RF power and vacuum, Spectrochim. Acta Part B 62 (2007) 370–377.
[34] J.H. Macedone, A.A. Mills, P.B. Farnsworth, Optical measurements of ion trajectories through the vacuum interface of an inductively coupled plasma mass spectrometer, Appl. Spectrosc. 58 (2004) 463–467.
[35] ANSYS FLUENT 12.0/12.1 Documentation, 2009.
[36] G. Gillson, G. Horlick, Comparison of atomic fluorescence and atomic emission spatial distribution profiles in the inductively coupled plasma, Spectrochim. Acta Part B 41 (1986) 1323–1346.
[37] N.N. Sesi, G.M. Hieftje, Studies into the interelement matrix effect in inductively coupled plasma spectrometry, Spectrochim. Acta Part B 51 (1996) 1601–1628.